Environment International 174 (2023) 107887

Contents lists available at ScienceDirect

Environment International

journal homepage: www.elsevier.com/locate/envint

Full length article

Identification of the roles of urban plume and local chemical production in ozone episodes observed in Long Island Sound during LISTOS 2018: Implications for ozone control strategies

Kaihui Zhao [a], Yonghua Wu [b], Jianping Huang [c,*], Guillaume Gronoff [d,e], Timothy A. Berkoff [d], Mark Arend [b], Fred Moshary [b]

[a] Yunnan Key Laboratory of Meteorological Disasters and Climate Resources in the Greater Mekong Subregion, Yunnan University, Kunming 650091, China
[b] Optical Remote Sensing Lab, the City College of New York (CCNY), New York, NY 10031, USA
[c] NOAA-NCEP Environmental Modeling Center and Lynker, College Park, MD 720740, USA
[d] NASA Langley Research Center, Hampton, VA 23681, USA
[e] Science Systems Applications, Inc. (SSAI), Hampton, VA 23681, USA

ARTICLE INFO

Handling Editor: Xavier Querol

Keywords:
O_3 pollution
Regional transport
Chemical reaction
O_3 precursor sensitivity
Long Island Sound

ABSTRACT

Long Island Sound (LIS) frequently experiences ozone (O_3) exceedance events that surpass national ambient air quality standards (NAAQS) due to complex driving factors. The underlying mechanisms governing summertime O_3 pollution are investigated through collaborative observations from lidar remote sensing and ground samplers during the 2018 LIS Tropospheric O_3 Study (LISTOS). Regional transport and local chemical reactions are identified as the two key driving factors behind the observed O_3 episodes in LIS. An enhanced laminar structure is observed in the O_3 vertical structure in the atmospheric boundary layer (i.e., 0–2 km layer) for the case dominated by regional transport. An O_3 formation regime shift is found in ozone-precursor sensitivity (OPS) for the O_3 exceedance event dominated by regional transport with NO_x-enriched air mass transport from the New York City (NYC) urban area to LIS. Furthermore, the Integrated Process Rate (IPR) analysis demonstrates that transport from the NYC urban area contributed 40% and 27.1% of surface O_3 enhancement to the cases dominated by regional transport and local production, respectively. This study provides scientific evidence to uncovers two key processes that govern summertime O_3 pollution over LIS and can help to improve emission control strategies to meet the attainment standards for ambient O_3 levels over LIS and other similar coastal areas.

1. Introduction

O_3 is a secondary pollutant generated by a series of photochemical reactions involving volatile organic compounds (VOCs) and nitrogen oxides (NO_x) under the favorable meteorological conditions such as strong solar radiation. Elevated levels of ambient O_3 have adverse effects on human health and vegetation growth (Westervelt et al., 2019; Zelm et al., 2016), as well as play a critical role in atmospheric chemistry (Verstraeten et al., 2015). The processes of constraining surface O_3 concentrations are extremely complex, and the complexity can be even higher in coastal megacities like New York. Therefore, quantifying the contributions of key processes continues to represent a great interest to the air quality research community and policy makers (Benjamin and Peter, 2011; Lin et al., 2012; Zheng et al., 2018).

Photochemical production and regional transport are critical to development of O_3 episodes (Verstraeten et al., 2015; Zhao et al., 2021a, b). Photochemical production heavily relies on the emissions of O_3 precursors. such as VOCs and NO_x, as well as their ratios ($VOCs/NO_x$). O_3 formation regimes can be further described using ozone-precursor sensitivity (OPS). Previous studies have shown that inappropriate emission control strategy could lead to an unexpected O_3 enhancement due to O_3-precursor nonlinearity (e.g., Ou et al., 2016; Xu et al., 2022). Regional transport is another important source accounting for the enhancement of surface O_3 (Derwent et al., 2004; Zhao et al., 2022). The O_3 precursors can be transported from highly polluted urban areas to downwind locations. Such urban plume can exacerbate the severity of air pollution and modify the VOC/NO_x ratios, making the air pollution chemistry even more complex (Zhao et al., 2022). Both chemical

* Corresponding author.
E-mail address: jianping.huang@noaa.gov (J. Huang).

https://doi.org/10.1016/j.envint.2023.107887
Received 17 November 2022; Received in revised form 8 March 2023; Accepted 15 March 2023
Available online 21 March 2023

production and transport are strongly influenced by meteorological conditions, such as strong solar radiation, high temperature, atmospheric boundary conditions, and winds (Liu et al., 2020; Zhao et al., 2019; Zhu and Liang, 2013). Extensive studies have demonstrated that both O_3 and its precursors can be transported horizontally or vertically, from upstream areas or the lower free troposphere, resulting in elevated O_3 level and O_3-precursor nonlinearity (Cooper et al., 2010; Luo et al., 2020; Zhao et al., 2021a,b; Zhao et al., 2022). Therefore, it is important to consider these processes when formulating anthropogenic emission control strategies to effectively mitigate O_3 NAAQS exceedance events.

New York City (NYC) is a coastal megacity with a population of more than 23.8 million people living in an area of nearly 35,000 km^2. Due to its strong anthropogenic emissions and coastal weather accompanied by land-sea breezes, it is more susceptible to O_3 pollution than other cities or regions (Karambelas, 2020; Ninneman et al., 2020; Zhang et al., 2020; Han et al., 2022). During summer months, O_3 exceedance events are frequently observed in NYC and its downwind coastal regions in Connecticut and Long Island. To understand O_3 pollution episodes in this region, the Long Island Sound Tropospheric O_3 Study (LISTOS) provided an excellent opportunity to explore the underlying mechanisms behind the O_3 episodes over LIS (Miller, 2017; Karambelas, 2020). Extensive measurements were conducted between June and September 2018 within the NYC metropolitan area and over Long Island Sound (LIS), including research aircrafts, O_3 lidars, wind-profiler, ceilometers, and surface in-situ observations. The LISTOS study revealed large spatial gradient variations of surface O_3 near the land–water interface, which were influenced by sea breeze during the study period (Zhang et al., 2020).

The causes of air pollution episodes in the NYC area have been investigated using numerical models and observations from the LISTOS field campaign. Studies by Couillard et al., (2021), Judd et al., (2020), Wu et al., 2021, Zhang et al., (2020) have identifiedland-water breezes, low-level jet, and regional transport as the primary factors contributing to O_3 enhancements. Han et al. (2022) further showed that sea breezes made dramatic impacts on ozone patterns in the NYC area. Torres-Vazquez et al. (2022) found that sound breezes and low-level jets play an important role in the transporting urban emissions and pollutants to the marine boundary layer in LIS and the coastal areas. Coggon et al. (2021) highlighed that the large impacts of volatile chemical products (VCPs) emissions in NYC on O_3 enhancement during heat waves. Additionally, Tao et al. (2022) investigated changes in O_3 formation chemistry using observed tropospheric column NO_2 and formaldehyde (HCHO) from satellite, airborne, and ground measurements in May-August 2018. Their findings suggest a transition toward a more NO_x-sensitive photochemical environment during high-ozone days in the NYC area.

In this study, Weather Research and Forecasting/Chemistry (WRF-Chem), version 3.9.1 is utilized to simulate the spatial and temporal characteristics of O_3 episodes with a fine grid spacing of 1.3 km. Ma et al. (2021) demonstrated that high-resolution simulations can improve the performance of air quality model in simulating high O_3 episodes. A variety of observational data from the LISTOS field campaign are used to better understand the mechanisms governing the O_3 episodes during Aug.5–9, 2018 over LIS. Two representative O_3 pollution events are presented to quantify the relative roles of regional transport and local photochemical production in their occurrences. The specific objectives of the study are to 1) quantify the contributions of individual processes to surface O_3 enhancement of two different types of O_3 exceedance events, 2) conduct a comprehensive assessment on the key driving factors governing the O_3 episodes over LIS, and 3) determine the changes in OPS over time and relate the changes to emission reduction strategies.

2. Methodology

2.1. Modeling system

The WRF-Chem version 3.9.1 was applied in this study. Three nested domains are employed in the simulations at grid-spacing of 13 km, 4 km, and 1.33 km with grid points of 110 × 85, 100 × 73, and 88 × 61 from the outermost domain (D1) to the innermost domain (D3), respectively (Fig. 1). The study focused on three surface O_3 monitoring sites in the coastal area of LIS: Westport, Flax Pond, and Eaton Neck. LIS is located at the northeast of NYC, the downwind area of NYC as the southwest winds prevail in NYC. Forty-six vertical layers from surface to the 50-hPa level were used with the lowest vertical layer about 40 m above the ground layer. All the physics parametrization schemes and the nudging configuration used in this study are the same as those used by Zhao et al. (2019). Atmospheric chemistry was simulated by the Regional Acid Deposition Model Version 2 (RADM2) (Stockwell et al., 1990). Details of the model configurations are provided in the Supplementary Material (**Table S1**).

The Final Operational Global Analysis data (FNL) with 1° horizontal resolution and 27 vertical levels from the surface to the 10-hPa level are used to generate initial and lateral boundary meteorological conditions to drive the WRF-Chem simulations. The Model for Ozone and Related Chemical Tracers Version 4 (MOZART-4/GEOS5) (Emmons et al., 2010) products are used to provide chemical initial and lateral conditions to the model simulations. Anthropogenic emissions from point, on-road mobile, non-road mobile, and area sources with a 4-km spatial resolution are provided by the 2014 National Emissions Inventory (NEI) developed by the U.S. Environmental Protection Agency (EPA) (Couillard et al., 2021; Judd et al., 2020; Wu et al., 2021; Zhang et al., 2020). Biogenic emissions are calculated using the Model of Emissions of Gases and Aerosols from Nature v2.1 (MEGAN) (Guenther et al., 2012). The land-use categories and distribution of NO_x and VOCs emissions over the NYC and LIS are depicted in Fig. 1 **and S1**. It is clear that the NYC metropolitan area was an important source of NO_x emissions contributed by human activities including traffic and industry, indicating a VOC-limited regime for emissions in NYC. On the other hand, as a suburban area, LIS has much less NO_x emissions but more isoprene emissions. When the prevailing wind was dominated by southwesterly, O_3 and its precursors were transported from NYC to LIS, exacerbating O_3 pollution and modifying the VOC-to-NO_x ratios and OPS.

Integrated Process Rates (IPR) is performed to quantify the relative contributions of physical processes and chemical reactions to the changes in O_3 concentrations during the events (Zhao et al., 2022). The changes in concentrations by individual processes are calculated at each integration time step and grid point throughout the simulations.

The ratio O_3/NO_y was proposed by Milford et al. (1994) as an indicator to represent O_3 formation potential. Since then, it has been widely used in modeling and observational studies to determine O_3 formation regimes (Liu et al., 2010; Sillman and He, 2002). According to the previous studies, areas with a ratio greater than 7 are characterized by NO_x-limited regime and otherwise defined as VOC-limited (Sillman and He, 2002).

2.2. Observational data

To improve understanding of O_3 formation over LIS, a large coordinated measurement campaign was carried out through joint collaboration among state and federal agencies and university research groups in the summer of 2018 LISTOS (https://www.nescaum.org/documents/listos). As listed in Table 1, a host of measurements were conducted to identify the relative roles of photochemical reactions and meteorological conditions during the O_3 exceedance events.

Hourly surface observations such as air temperature, relative humidity, wind speed, wind direction, and air quality data were collected synchronously at five sites across the NYC and surrounding regions. The information about the sites and the measured variables can be found from Fig. 1 and Table 1. During the campaign, surface O_3 was routinely measured at the Air Quality Stations (CCNY, Flax Pond, Westport) operated by the US Environment Protection Agency (EPA), with a measurement uncertainty of approximately ± 4 ppbv, as indicated by

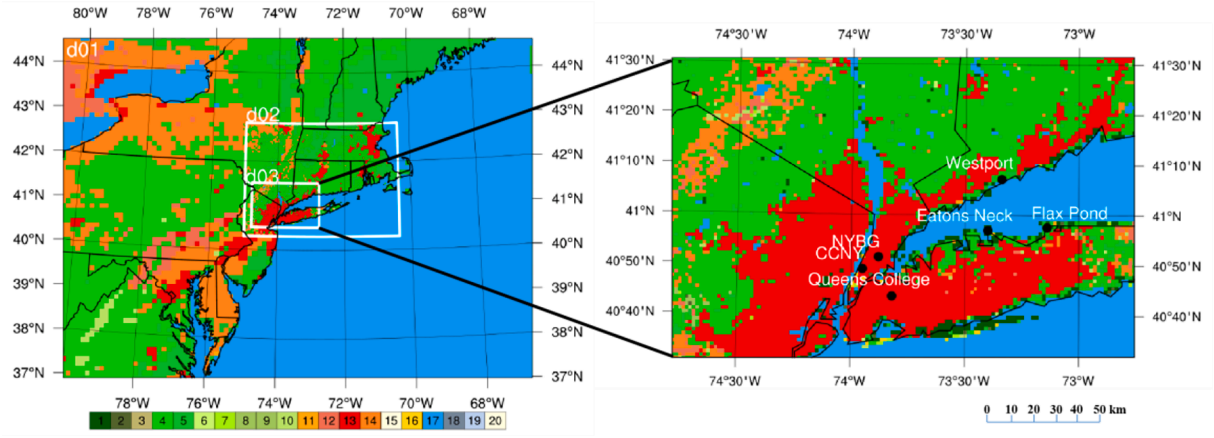

Fig. 1. Settings of three domains in WRF-Chem modeling system and meteorological and air quality sites in the NYC and Long Island areas. Detailed land-use categories are as follows: 1: evergreen needleleaf forest; 2: evergreen broadleaf forest; 3: deciduous needleleaf forest; 4: deciduous broadleaf forest; 5: mixed forests; 6: closed shrublands; 7: open shrublands; 8: woody savannas; 9: savannas; 10: grasslands; 11: permanent wetlands; 12: croplands; 13: urban and built-up land; 14: cropland/natural vegetation mosaic; 15: snow and ice; 16: barren or sparsely vegetated; 17: water; 18: wooded tundra; 19: mixed tundra; and 20: barren tundra.

Table 1
A Summary of monitoring sites locations and data used in this study.

Site	Latitude (North)	Longitude (West)	Measured variable	Elevation (AGL)	Measurement
Eatons Neck	40.95°	73.4°	O_3, Attenuated backscatter	5 m	Surface O_3 observation, ceilometer
CCNY	40.82°	73.95°	O_3, NO_2 Attenuated backscatter	15 m	Surface air quality and meteorological observation
Flax Pond	40.96°	73.14°	O_3, NO_x,	4 m	Surface air quality observation
NYBG	40.86°	73.88°	O_3	15 m	Surface air quality observation
Queens College	40.73°	73.82°	O_3, NO_x	5 m	Surface air quality observation
Westport	41.12°	73.34°	O_3 and wind profile	3 m	Surface air quality observation, O_3 Lidar, wind lidar

zero drift during 12–24 h duration (Duvall et al., 2021). The Model 202/205 Dual Beam Ozone Monitor (2B-Tech) was used to measure O_3 at Eatons Neck with a precision of 1.0 ppb (https://www.twobtech.com/model-205-ozone-monitor.html). It has been approved by the EPA as a Federal Equivalent Method (FEM). However, the TAPI Model 500U sensor overestimates NO_2 by approximately 10% due to the conversion of total odd nitrogen to NO by molybdenum oxide catalysts (McClenny et al., 2002).

Various remote sensing instruments were used to characterize vertical distributions of attenuated backscatter, wind speed and direction, and O_3. These instruments include the Vaisala CL-51 and CL-31 ceilometers, the Leosphere WindCube 200S coherent Doppler wind lidar, City College of New York (CCNY) aerosol lidar, and the NASA Langley Mobile O_3 Lidar (LMOL).

The ceilometer measured the attenuated backscatter at a laser wavelength of 910 nm with 10 m × 770 samples a data collection interval of 15 s, which can be used to determine the planetary boundary layer height (PBLH). A wavelet covariance transforms (WCT) method was used to calculate the PBLH based on vertical gradient variation of aerosol backscatter profiles (Gan et al., 2011). The PBLH was determined by locating sharp gradient or minimum gradient in the ceilometer-measured attenuated backscatter profiles. The uncertainty stems from the signal noises, aloft aerosol layer and low-level cloud, thus a quality control and quality assurance (QA/QC) process is applied to remove those outliers (Münkel, et al., 2011). Besides, a coherent Doppler Wind Lidar (WindCube 200s) was installed in Westport (West coast of Long Island Sound) to measure wind profiles with a range-gate spacing of 25–50 m and a sampling frequency of 10 s. A vertically pointing eye-safe laser (wavelength 1.54 μm with a repetition rate of 10 kHz) was used to measure wind velocity and direction (Brotzge et al., 2020). The precision of the wind profile is in the range of 0.2 m•s^{-1}-0.5 m•s^{-1} (Brotzge et al., 2020). The NASA Langley Mobile Ozone Lidar (LMOL) was deployed at Westport to measure O_3 vertical structure using the differential absorption principle at the UV wavelength pair of 287 and 292 nm (De Young et al., 2017). The O_3 profiles were retrieved with a 5–10 min average from LMOL (Gronoff et al., 2019). The LMOL shows great agreement with the ECC ozonesondes, with an overall mean bias of 1–4 ppbv for the altitude range 3–10 km (De Young et al., 2017). Hourly-averaged O_3 profiles were used to evaluate the WRF-Chem predictions of O_3. Overall, the synergistic use of ceilometer, wind lidar, and O_3 lidar observation provided a unique opportunity to verify the model performance and better understand the underlying mechanisms governing the O_3 episodes over LIS.

3. Result and Discussion

3.1. General characteristics of O_3 episode in August 2018

The time series of hourly averaged O_3 concentrations at CCNY, Flax Pond, and New York Botanic Garden (NYBG) are presented in **Fig. S2**. The hourly maximum O_3 reached 85.0 ppbv on Aug. 6 and 86.8 ppbv on Aug. 8. **Fig. S3** illustrates a time series comparison of observed 2-m temperature, relative humidity, wind speed, and wind direction at the site CCNY (see the locations in Fig. 1 and Table. 1) on Aug. 5–9, 2018. During this period, the hourly-average maximum temperature was above 32.5 °C in the NYC areas, which met the heatwave definition criteria (Robinson, 2001; https://www.weather.gov/okx/excessiveheat). As illustrated in Fig. S3**d**, the prevailing wind direction was southwest with a wind speed range of 2–5 m s^{-1} which transported air pollutants from NYC areas to the LIS.

O_3 episodes are generally associated with the favorable synoptic systems (Zhang et al., 2020; Zhao et al., 2021a,b). On Aug. 6, a high-pressure system centered in the Atlantic Ocean and a low-pressure system located northeast of the high-pressure system(Fig. 2**a**) resulted in southwest winds with relatively high wind speed(i.e., 10 m/s), due to the large pressure gradient between these two systems (**Fig. S6**). In NYC,

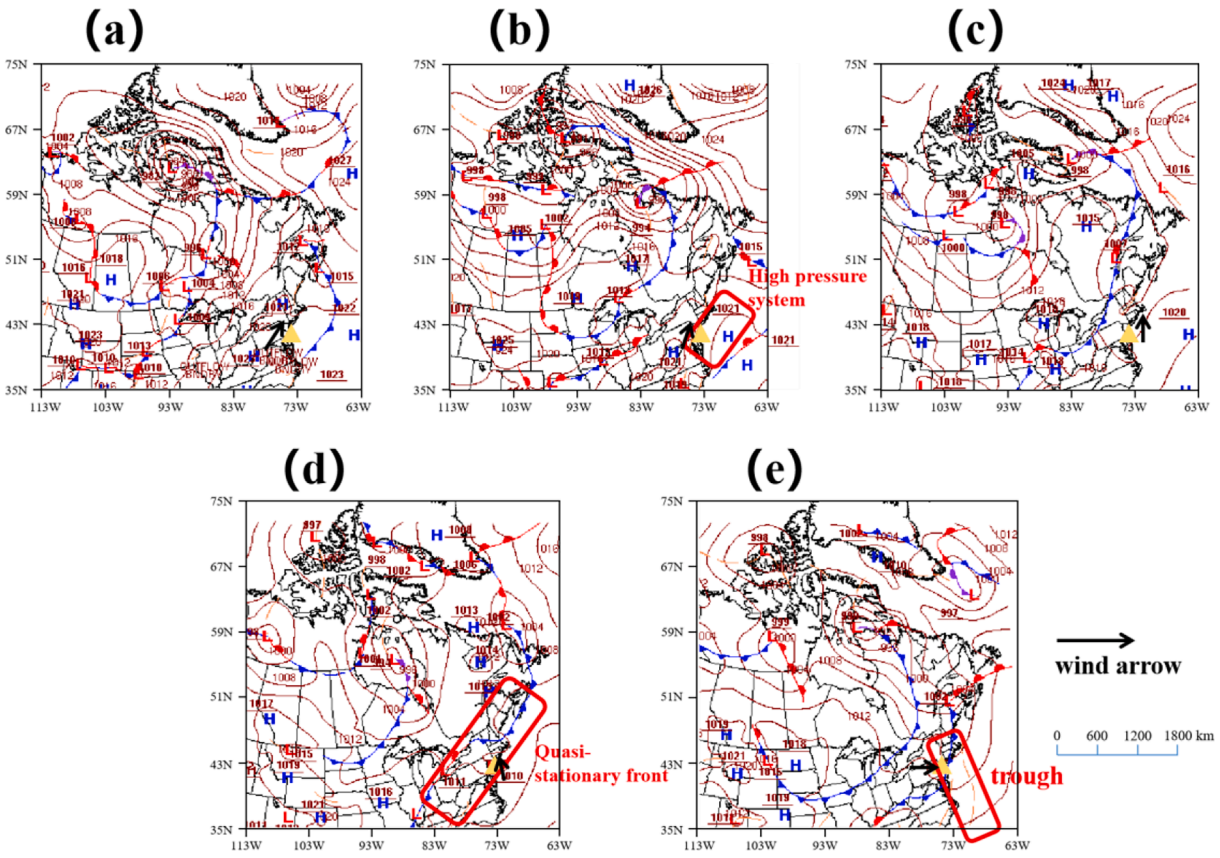

Fig. 2. Surface weather charts at 07 EST on (a) 5, (b) 6, (c) 7, (d) 8, (e) 9, Aug. 2018 (yellow triangle: New York City) (https://www.wpc.ncep.noaa.gov/archives/web_pages/sfc/historic_sfc_archive.php). (For interpretation of the references to colour in this figure legend, the reader is referred to the web version of this article.)

the daily maximum temperatures reached 35.0 °C (Fig. S3). At the same time, a low pressure system and a high pressure system were observed over Atlantic Ocean and over Pennsylvania, respectively. The prevailing winds were southwesterly, facilitating horizontal O_3 transport from NYC to LIS. On Aug. 8, a quasi-stationary front approached LIS from the northwest, accompanied by high temperatures, weak wind speed, and strong sunlight, which were conducive to local photochemical reaction and accumulation. Owing to weak background winds (i.e., 6 m/s), regional transport played a minor role in O_3 pollution, which was mainly controlled by local photochemical production (Fig. S9). On Aug. 9, the transverse trough shaped vertically and the center of the low-pressure moved northward, resulting in LIS being located behind a cold front and experiencing heavy precipitation.

3.2. *Two representative O_3 enhancement episodes*

Two significant O_3 exceedance events were observed with the 1–5 min averaged O_3 concentrations exceeding 98.2 ppbv on Aug. 6 and 115.2 ppbv at Westport on Aug. 8, 2018, respectively. The MDA8 O_3 reached 77.5 ppbv on Aug. 6 and 85.0 ppbv on Aug. 8, exceeding the NAAQS for O_3. As depicted in Fig. 3, a remarkable difference in O_3 diurnal characteristics between these two days was noticed.

A bimodal structure was observed at all sites, with twin peaks appearing at 12:00–14:00 and 16:00–18:00 Aug. 6, 2018. In particular,

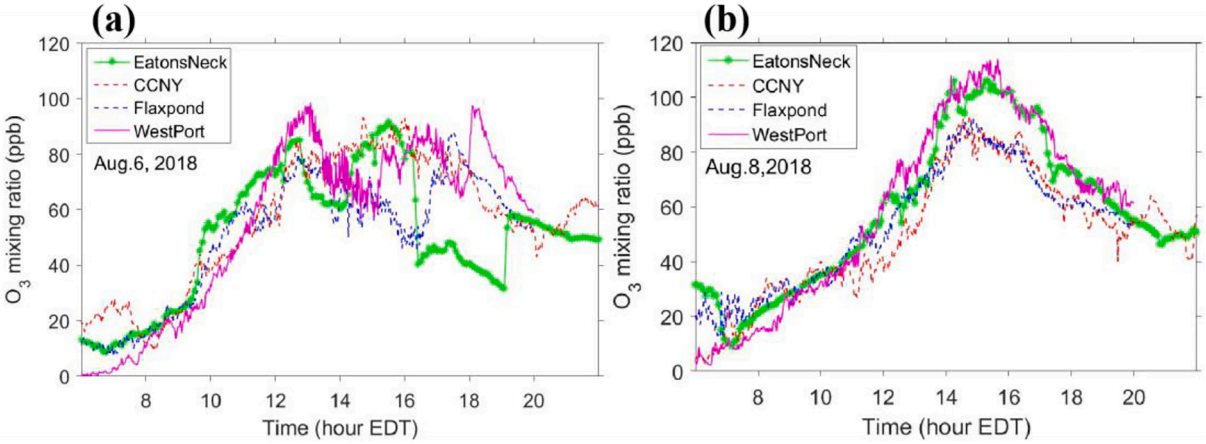

Fig. 3. O_3 concentration (1–5 min average) at the ground stations in NYC and LIS areas on (a) Aug. 6 (b) Aug. 8, 2018 (1-min Ave at Westport, Flax Pond, and CCNY, 5-min Ave at Eatons Neck).

at the Westport site, three O_3 peaks were observed at 13:00, 16:00 and 18:00 EDT, respectively. A time lag of approximately one hour between these four sites were observed for the second peak time, indicating an impact of cloud and regional transport. As shown in **Fig. S4**, a low-level cumulus was observed at 1.8 km on Aug. 6, which attenuated solar radiation and changed the diurnal structure of O_3, resulting in the low value at 13:00–14:00 EDT. The Satellite MODIS (Terra, 14:30 UTC overpass time, and Aqua, 18:03 UTC overpass time) RGB images on Aug. 6, 2018, clearly indicate the broken clouds in the NYC area (**Fig. S5**). The second peak O_3 value occurred at 18:00–20:00 EDT, when photochemical reactions tended to be inactive but wind velocity exceeded 8 m/s (**Fig. S6**), indicating the impact of regional transport. On the other hand, surface O_3 exhibited a unimodal pattern with its peak at 15:00–16:00 EDT on Aug. 8, following the solar radiation variation pattern, and a minimum value between 0600 and 0700 LST due to NO titration effect, suggesting that the O_3 episode was dominated by local photochemical reactions.

To investigate the two representative O_3 episodes further, we compared NO_x simulations at the first model level (about 40 m above ground level) with air quality measurements near surface to evaluate the model performance (see Fig. 4). As indicated by the dash blue boxes, the NO_x level on Aug. 6 was much higher than that on Aug. 8 at 07:00 EDT (58.0 ppbv vs. 41.2 ppbv at Queens College and 15 ppbv vs. 10 ppbv at Flax Pond). Since the local emission intensity was relatively stable on consecutive days, the elevated NO_x levels, as an important sources of O_3 precursors, can be transported from urban to the downwind areas. Higher amounts of NO_x, as a critical O_3 precursor, favor the transition of OPS from NO_x-limited to VOC-limited.

The model had a good performance in NO_x simulation, with correlation coefficient (R) of 0.68 at Queens College and 0.85 at Flax pond. A comparison of observed versus simulated O_3 concentrations in the three sites is also shown in **Fig. S2**, and a statistical evaluation of O_3 simulation is presented in **Table S2**. Overall, the model exhibited good simulation performance of hourly O_3 at these sites during the O_3 episode, with R of 0.84–0.92, RMSE of 4.6–10.3 ppbv, and MB of −0.8–5.3 ppbv. The uncertainties of O_3 precursor emissions could be one of main reasons for the underprediction of the O_3 peak. For instance, the lower simulated NO concentration weakened the NO titration, which led to the over-prediction of O_3 during the nighttime. Coggon et al. (2021) also reported that volatile chemical products (VCPs) emissions in NYC exerted large impacts on O_3 simulation. We also make a comparison of simulated surface temperature, relative humidity, wind speed, wind direction with observations at CCNY during Aug. 5–9, 2018, as shown in **Fig. S7**. The statistical evaluation of simulated surface meteorological variables is listed in **Table S3**. Overall, the model was able to capture diurnal variation of surface meteorological variables, but underestimated temperature peak levels and overestimated wind speed, which may lead to under-predictions of the daytime O_3 peaks.

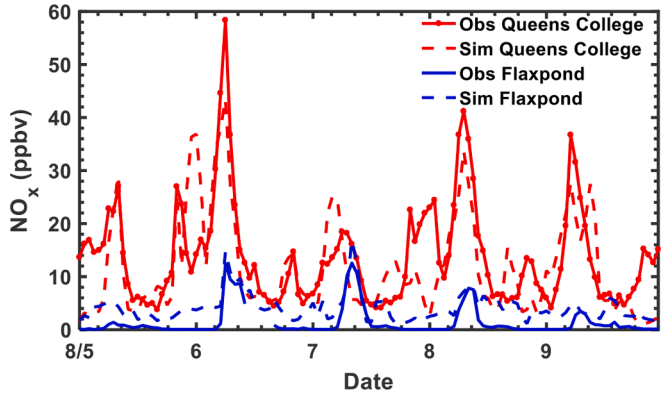

Fig. 4. A comparison of observed with simulated hourly NO_x concentrations at the ground stations in NYC (QC) and LIS (Flax Pond) areas during Aug. 5–8, 2018.

In summary, the biases in O_3 predictions could be attributed to by a variety of factors such as inaccuracies in anthropogenic emissions inventories (Zhao et al., 2022), biogenic emissions (Zhao et al., 2019), meteorological fields (e.g., PBLH, eddy diffusivity, winds, clouds, temperature), dry deposition (Shen et al., 2011), gas-phase chemical mechanisms (Gupta and Mohan (2015), chemical initialization constraint (Ma et al., 2021), and model resolution (Torres-Vazquez et al., 2022), etc.

3.3. *Mechanisms governing the O_3 episodes over Long Island Sound*

As discussed in the previous section, the two representative cases were dominated by regional transport and local photochemical reactions, respectively. In this section, we further investigate the underlying mechanisms that were responsible for these two O_3 episodes observed over LIS.

3.3.1. *Case A on August 6: Dominated by regional transport*

The NASA LMOL was used to measure O_3 with a 10-min temporal resolution and a vertical resolution that ranges from 50 m near the ground to 1 km at maximum altitude, utilizing an adaptive resolution scheme (Gronoff et al., 2021). The vertical height covers a range from 100 m above ground level (AGL) to middle troposphere. To evaluate the model performance, the original lidar data was interpolated to 21 model levels in the range of 6.2–7000 m and then averaged on an hourly basis.

Fig. 5**a–b** depict the time-height cross-sections of observed and simulated O_3 at Westport, a coastal site along LIS, respectively. Due to the UV light from the Sun, the lidar signal was noisy during noon local time, which prevented the retrieval of O_3 at altitudes above approximately 4 km, as shown by the lack of data above these altitudes in Fig. 5**a**. Howver, despite this limitation, the WRF-Chem model was able to reproduce the diurnal variations of O_3 vertical distributionwell.

As discussed above, the observational data reported severe surface O_3 pollution on Aug. 6, with multi-peak diurnal variations, indicating the potential impact of regional transport (Fig. 3**a**). The time-height cross-section in Fig. 5**a** provides further insightes into the O_3 distrubiton, showing a significant O_3 enhancement layer with concentrations of 60 ~ 100 ppbvbetween surface and 2 km, gradually increasing from 13 EDT to 19 EDT. The blue box in Fig. 5**c** highlights the strong vertical wind velocity detected by Doppler wind lidar, which exceeded −1.5 m/s from 15 EDT to 19 EDT, facilitating the vertical transport of O_3 from the upper level. The strong backscatter signal indicates that the aerosol plumes were transported from the free atmosphere (2.5 km AGL) downward to the surface layer, aggravating the surface air pollution (Fig. 5**d**). However, a low-level cumulus was observed by the ceilometer at 4 km AGL from 15 EDT to 16 EDT on Aug. 6, significantly reducing the solar radiation reaching the surface and weakening the local O_3 photochemical reactions.

The vertical distributions of horizontal wind speed and direction measured by Doppler wind lidar during 18 EDT-20 EDT are shown in **Fig. S6**. A low-level jet (LLJ) was observed at the height of about 1.5 km AGL after 18 EDT which is responsible for the subsidence area shown in Fig. 5**c**. The high southwest wind speed (greater than 8 m/s) would led to the O_3-enriched air aloft being entrained from the residual layer down to the surface layer. Meanwhile, another strong wind band was noticed above the ground. Such a strong jet stream was conducive to O_3 dispersion and sedimentation, leading to the attenuation of surface O_3. Therefore, the lidar-observed O_3 enhancement at Westport was possibly associated with regional transport and road transport from the NYC urban area.

Apart from regional transport, photochemical reactions are another factor driving O_3 formation. At 10 EST, the hourly maximum O_3 reached 55.0 ppbv (Fig. 6**a**). As solar radiation increased, the O_3 enhancement area developed as a southwest-northeastern band along the coastal region, with the O_3 maximum center located at LIS at 14 EST (Fig. 6**b**). A

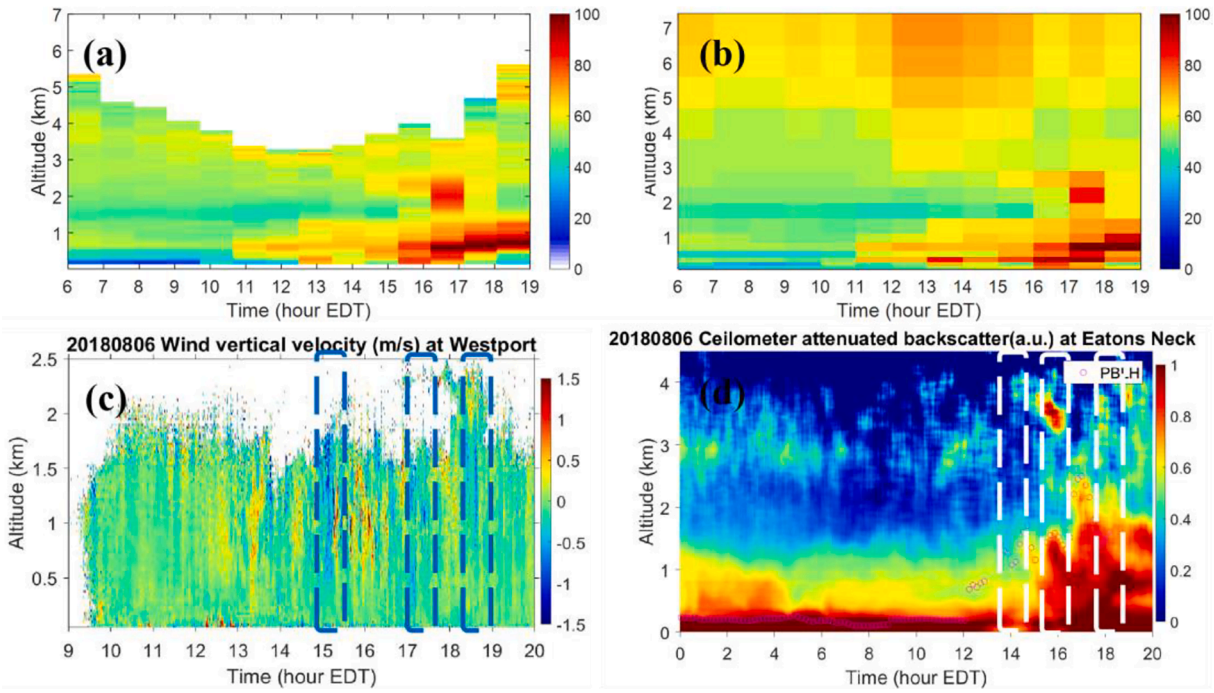

Fig. 5. Time-height cross sections of (a) observed, (b) simulated O_3 (O_3, ppbv), (c) observed vertical wind velocity ("+" upward wind, "-" downward wind) at Westport, (d) ceilometer-measured attenuated backscatter ($km^{-1}{\cdot}sr^{-1}$) at Eatons Neck, New York state, on Aug. 6, 2018.

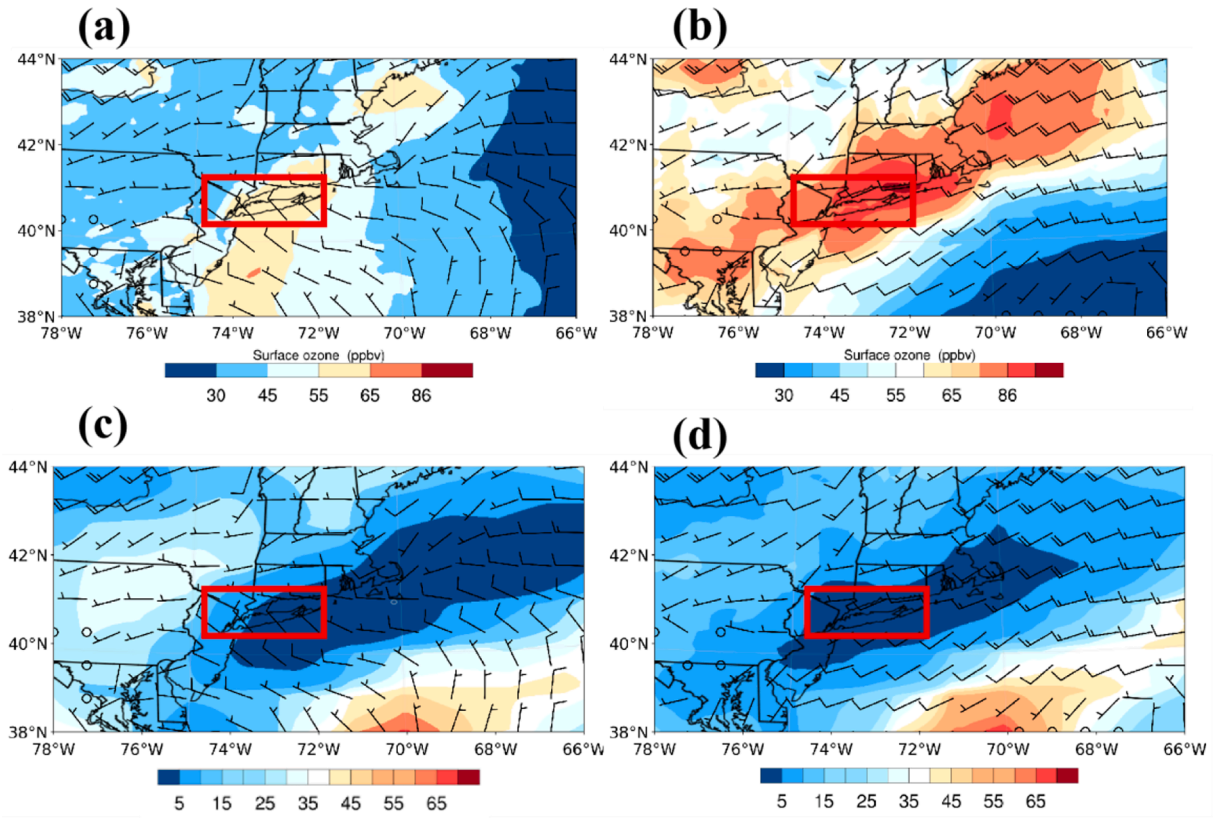

Fig. 6. WRF-Chem's predictions (a,b) surface O_3 and (c,d) O_3/NO_y at 10:00 EST and 14:00 EST on 06, Aug, 2018. The studying area is highlighted in red boxes. (For interpretation of the references to colour in this figure legend, the reader is referred to the web version of this article.)

large amount of NO_x was transported to LIS and the concentration was elevated to 58 ppbv at Queens College and 15 ppbv at Flax Pond (Fig. 4).

As mentioned earlier, regional transport of NO_x may potentially impact OPS. This motivates further characterization of OPS variations during this event. The spatial distribution of OPS was investigated using O_3/NO_y, a widely-used indicator (Liu et al., 2010; Sillman and He, 2002). A comparison of simulated vs. observed hourly NO_y at Flax Pond is presented in **Fig. S8**, and the statistical parameters are provided in

Table S4 to evaluate the model performance. Overall, the model had a reasonable performance in simulating NO_y with correlation coefficient (R) of 0.58 and mean bias (MB) of 3.6 ppb. In comparison with simulated O_3, the ratios of O_3/NO_y on Aug. 6, which were lower than 5, agreed well with the O_3 enhancement area, indicating that O_3 formation was dominated by the VOC-limited regime over the NYC and LIS areas (Fig. 6**c,d**). Compared to LIS, high vegetation coverages were noticed in central and eastern LIS, which would emit a large amount of biogenic VOCs such as isoprene and monoterpene, important precursors of O_3 formation. With the increase in NO_x concentration, the NO_x-limited regime transitioned to VOC-limited and O_3 mixing ratio increased sharply in response to NO_x enhancement. Our analysis highlighted that the regional transport not only increased the O_3 level but also strengthened the chemical reactions by decreasing the VOC-to-NO_x ratio, leading to variations in OPS. Thus, it is necessary to consider the impact of long-range transport on OPS from neighboring cities for refining O_3 control strategy.

3.3.2. *Case B on Aug 8: Dominated by local chemical production*

Another severe O_3 episode with the highest hourly O_3 exceeding 90 ppbv at both sites was observed on Aug. 8. The typical single peak structure of O_3 and relatively lower NO_x level suggest a dominate role of local photochemical reactions in the development of the episode (Fig. 3**b and 4**).

A pool of O_3 with a concentration greater than 80.0 ppbv was observed through O3 lidar below 1.5 km altitude (Fig. 7**a**). The simulated O_3 showed very good agreement with the lidar observation below 2 km, but slightly underestimated the peak O_3 levels (Fig. 7**b**). Hourly-averaged O_3 reached 91.4 ppbv at 1.1 km altitude from 15 to 17 EDT, which exceeded the NAAQS for O_3. The time-height cross-section shows a peak of O_3 in the boundary layer at noon, coinciding with the daily maximum solar radiation. This is mainly due to local photochemical production and transport of O_3 from the NYC urban area. After 18 EDT, a layer with O_3 concentration higher than 80.0 ppbv remained at the height of 1 km above ground level, indicating that the local chemical production played a significant role in the exceedance of NAAQS for O_3.

Fig. 7**c** presents a time-height cross-section of vertical wind speed measured by the Doppler wind lidar. Ascent motions were observed at 15 EDT, 16 EDT, and 19 EDT, which contributed to the formation of a high-O_3 layer at 1 km. In contrast, at 18 EDT, a strong subsidence movement was observed, indicated by negative vertical wind speed (vertical velocity < -1.5 m/s). The subsidence movement was caused by a strong southwest jet (wind velocity greater than 10 m/s) located between 1.5 and 2 km (**Fig. S9**), resulting in the O_3-enriched air mass descending from the 7 km to 1 km with O_3 concentrations reaching 60.0 ppbv at 18 EDT (Fig. 7**b**). Fig. 7**d** shows the spatiotemporal variations of the attenuated backscatter at Eatons Neck. The low-level clouds at 1.5 km significantly reduced the solar radiation, leading to a decrease in surface O_3 after 18 EDT.

A similar O_3 hot-spot pattern along southwest-northeast direction was noticed with 10 ppbv higher than that on Aug. 6 (Fig. 8**a,b**). The hourly O_3 concentration had increased by 10–20 ppbv during 10–14 EST. OPS achieved a relatively high O_3/NO_y ratio (i.e., 15), indicating the NO_x-limited regime of O_3 formation at LIS (Fig. 8**c,d**). This is consistent with the fact that Long Island was well covered vegetation and NO_x emissions were low, the regional transport may only marginally contribute to the O_3 enhancement.

Overall, both O_3 and O_3 precursors (i.e., VOCs and NO_x) can be transported from the NYC urban area to LIS. The O_3-enriched air transported from NYC could exacerbate O_3 pollution over LIS. Meanwhile Long Island has a higher vegetation coverage than NYC, which leads to higher emissions of isoprene and monoterpene (Geng et al., 2011). Thus, LIS was dominated by the NO_x-limited regime. In comparison, NO_x emissions were emitted from power plants, transportation, and fossil fuel combustion activities over the NYC. As a result, NO_x-enriched air transported from NYC could decrease the VOC-to-NO_x ratio, thus shifting the OPS toward the VOC-limited regime.

As OPS varies with different scenarios, we recommend a dynamic O_3 control strategy for LIS with priority given to controlling either VOC or NO_x emission sources depending on which factor dominates. When the NO_x-enriched air is transported to LIS, a VOC-focused strategy is recommend to effectively lower the O_3 levels. In contrast, NO_x emission reduction should be prioritized when the local photochemical reactions dominate. Overall, the impact of O_3 and its precursor transport from the

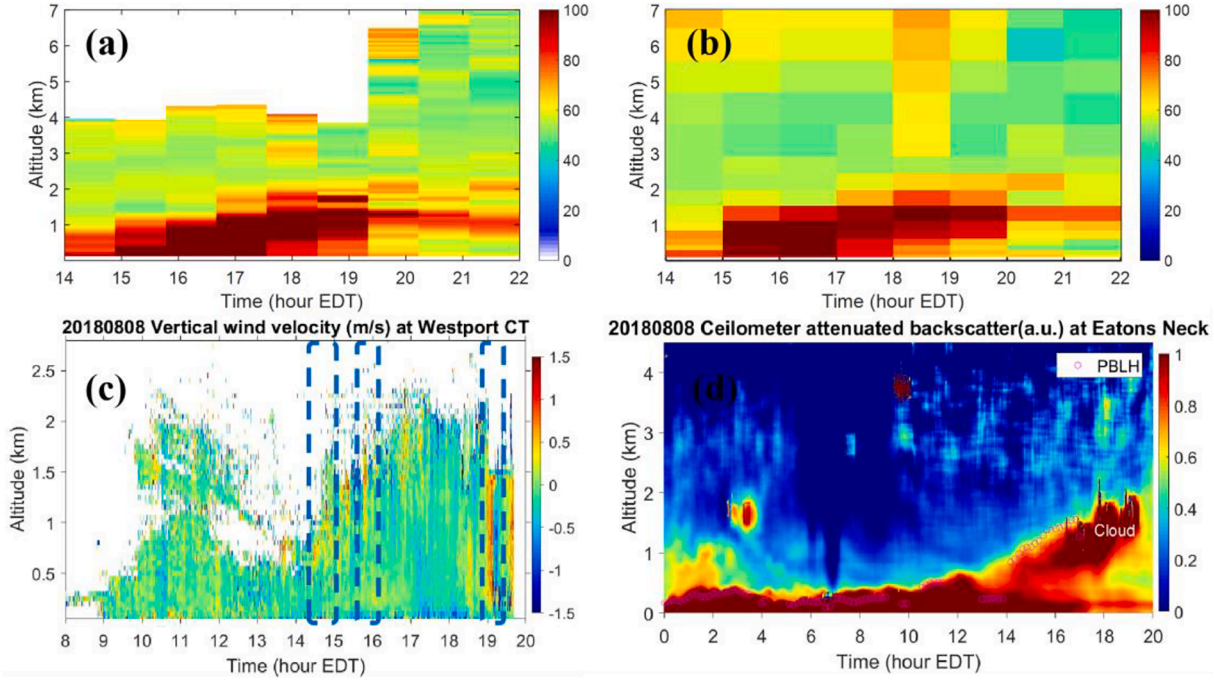

Fig. 7. Time-height cross section plot of (a) observed, (b) simulated O_3 (O_3, ppbv), (c) observed vertical wind velocity at Westport, (d) ceilometer-measured attenuated backscatter ($km^{-1}\cdot sr^{-1}$) at Eatons Neck on Aug. 8, 2018.

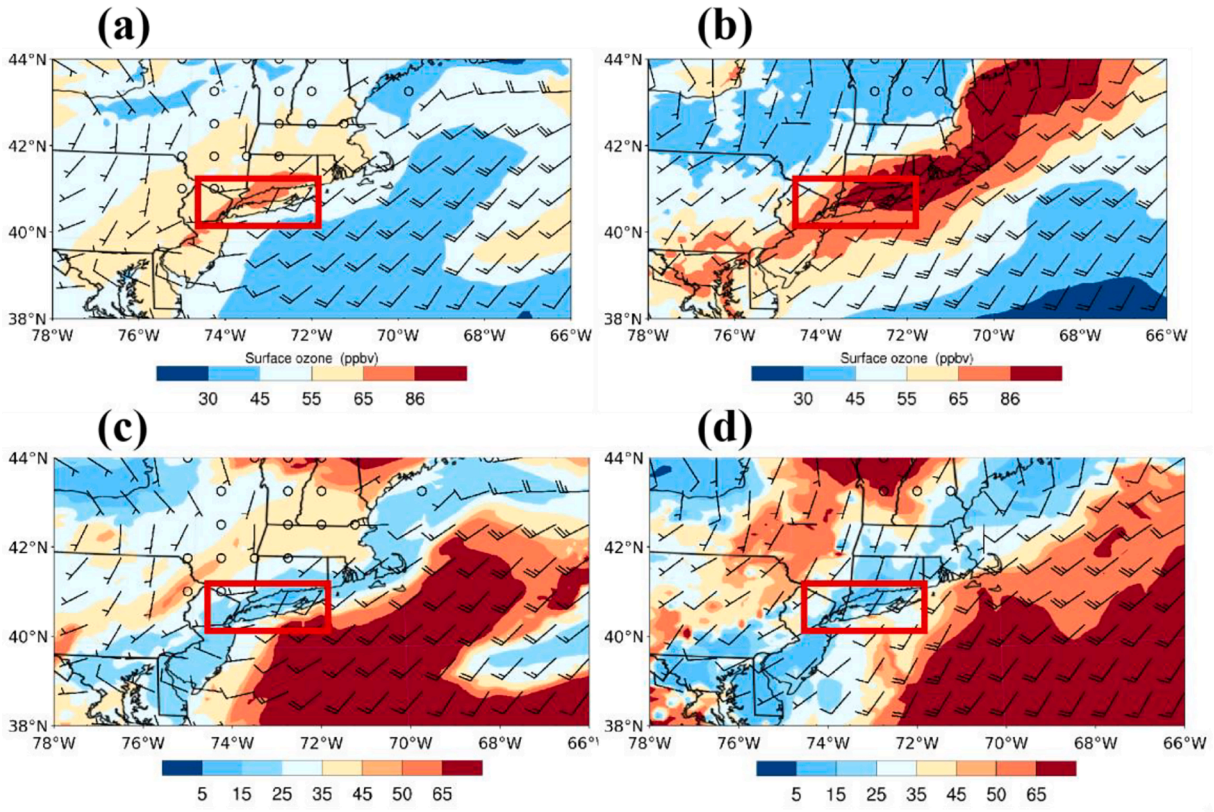

Fig. 8. WRF-Chem's predictions (a,b) surface O_3 and (c,d) O_3/NO_y at 10:00 EST and 14:00 EST on 08, Aug. 2018. The studying area is highlighted in red boxes. (For interpretation of the references to colour in this figure legend, the reader is referred to the web version of this article.)

NYC area to LIS needs to be considered when emission control strategies are implemented to mitigate O_3 pollution effectively.

In summary, the detected subsidence drived by the stronger low-level jet and the presence of clouds on Aug. 6 were responsible for the difference between these two representative O_3 episodes. Moreover, the variation in OPS is another important factor accounting for the large differences observed.

3.4. Quantification of different processes in the two representative O_3 episodes

To better quantify the contribution from individual process to the O_3 exceedance events at LIS, we calculate the hourly relative contributions from chemical and physical processes to the total O_3 budget through an IPR analysis. The IPR analysis results were obtained from the WRF-Chem simulations at the nearest point to the Eatons Neck.

As shown in Fig. 9, chemical processes were found to be important to O_3 formation in both cases. The produced O_3 through chemical reaction at Eatons Neck and studying time period was 4.6 ppbv·hr^{-1} on Aug. 6 and 6.2 ppbv·hr^{-1} on Aug. 8, respectively. However, due to the low-level clouds, the contribution of chemical reaction significantly reduced to 0.4 ppbv·hr^{-1} on Aug. 9 at Eatons Neck.

Physical processes including horizontal advection and vertical transport posed positive contributions to O_3 enhancement on 5, 6, and 8 Aug. The contributions of regional transport to surface O_3 on Aug. 6 was much higher than that on Aug. 8 (3.8 ppbv·hr^{-1} vs. 1.2 ppbv·hr^{-1}). Our results further proved that regional transport and local chemical reaction are the key factors for the development of episodes observed on

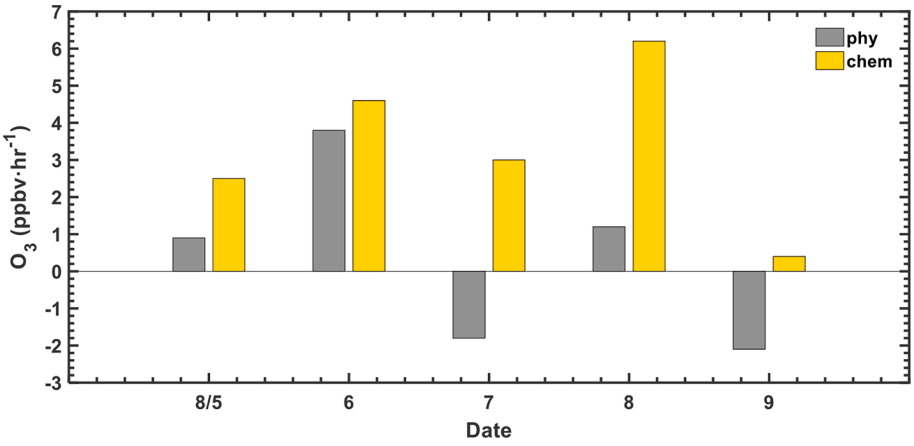

Fig. 9. Contribution of physical and chemical process to O_3 changes at Eatons Neck calculated through IPR analysis.

Aug. 6 and 8, respectively.

As introduced in Section 1, air pollutants from NYC were transported to the downwind areas, exerting an important impact on air quality over LIS. Thus, a sensitive study was conducted without anthropogenic emissions to quantify the relative contributions from the NYC area to the air quality over LIS.

In order to quantify the relative contribution of regional transport from the NYC area to LIS, a sensitive study was conducted without any anthropogenic emission reduction applied to NYC. The results indicated that the regional contribution of O_3 from the NYC area (urban emissions) varied greatly for the two representative O_3 enhancement episodes. During the daytime (07:00–18:00 EDT), the O_3 contribution from the NYC area to Eatons Neck ranged from 8.1 to 27.4 ppbv per-hour on Aug. 6, accounting for 5.9–40.0% of the total O_3 levels (Fig. 10). This indicated the significant impact of transport from NYC in elevating O_3 ambient levels. On the other hand, the NYC area only contributed 0.6–12.6 ppbv per-hour on Aug. 8, which only explained 1.7–27.1% of O_3 episode. Therefore, our results underscore the necessities in expanding the emission reduction area to offset the impact from the NYC area if the regional transport dominates.

It is worth noting that the factors influencing surface O_3 budget are more complex for LIS, a coastal area, which is affected by local-scale circulation such as sea breezes and regional transport from other upwind areas. Hence, further sensitive studies are necessary to identify the contributions from other source regions to LIS and their impact on OPS variations.

4. Conclusions and implications

Summertime O_3 pollution poses a significant risk to millions of people living in NYC and surrounding areas. In the summer of 2012, the LISTOS field campaign was carried out with a synergistic combination of multi-source observations and model studies to better understand the underlying mechanisms responsible for O_3 exceedance events over LIS.

This study aimed at to better understand the mechanisms driving summertime O_3 pollution by utilizing the WRF-Chem model and a collection of 3D observational data from LISTOS 2018 campaign. High-resolution simulations were able to capture the spatiotemporal variations of O_3, NO_x, NO_y, meteorological variables, and vertical structures of air pollutants during episode development. The study identified two representative O_3 enhancement events dominated by regional transport and local photochemical reactions, respectively.

When the regional transport was dominant, the study found that O_3 laminar structure with concentration of 60 ~ 100 ppbv within the atmospheric boundary layer was transported down to the surface layer through subsidence movement. On the other hand, when local photochemical reactions were the dominant contributions to O_3 enhancement, a pool of O_3 with concentration higher than 80 ppbv was formed below the height of 1 km.

The study found a significant variations in OPS associated with regional transport. Higher NO_x emissions from power plants, transportation, and fossil fuel combustion activities over the NYC decreased the VOC-to-NO_x ratio, shifting the OPS toward the VOC-limited regime. The study recommends adjusting the O_3 control strategy for LIS dynamically based on varying OPS.

IPR analysis indicates that photochemical reactions positively contribute to the development of the two representative O_3 exceedance events while the physical processes show great variations. On Aug. 6, physical processes including horizontal advection and vertical transport posted a maximum contribution of 3.8 ppbv·hr^{-1} to O_3 enhancement. Sensitivity studies with emission reduction scenario demonstrated that the O_3 formation was highly related to regional source contributions from NYC with hourly O_3 contribution reaching 27.4 ppbv on Aug. 6 and 12.6 ppbv on Aug. 8, accounting for 40% and 27.1% of the total production, respectively.

This study highlights the importance using a high resolution for simulating O_3 episodes, especially the O_3 vertical structure, over LIS and other coastal areas worldwide. Regional transport and local chemical reactions are identified as two key factors responsible for O_3 enhancement from multi-source observations for LIS. The large contribution from the NYC area underscores the importance of strengthening the regional synergistic emission reduction strategy to mitigate ambient O_3 pollution over LIS. The results also emphasize the need to adopt a dynamic O_3 control strategy for LIS based on OPS, particularly in cases where local O_3 levels are significantly influenced by non-local sources.

CRediT authorship contribution statement

Kaihui Zhao: Methodology, Investigation, Software, Validation, Formal analysis, Writing – original draft. **Yonghua Wu:** Supervision, Validation, Formal analysis, Writing – review & editing. **Jianping Huang:** Supervision, Conceptualization, Methodology, Writing – review & editing. **Guillaume Gronoff:** Methodology, Writing – review & editing. **Timothy A. Berkoff:** Software, Resources. **Mark Arend:** Resources.

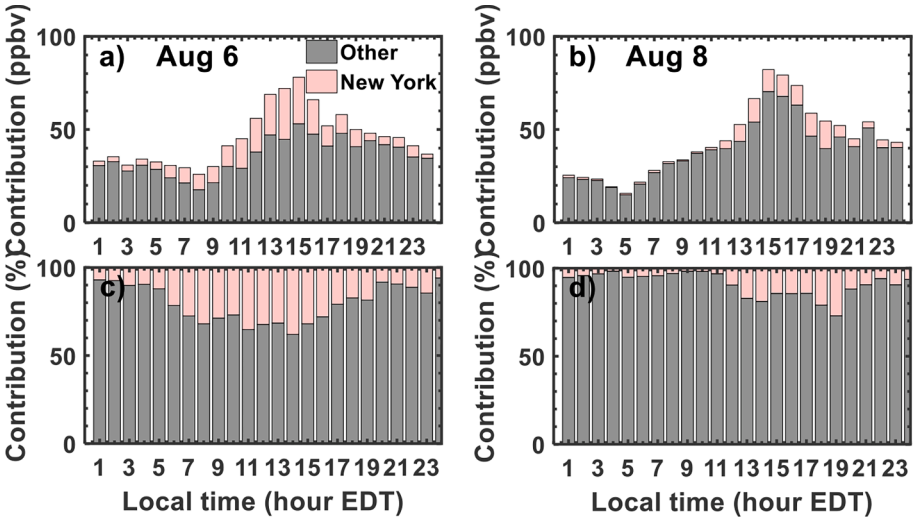

Fig. 10. Daily variations of contribution (ppbv) from the sensitivity analysis from NYC (pink bar) and other areas (grey bar) to Eatons Neck on (a) Aug. 6 and (b) Aug. 8, as well as relative contribution on (c) Aug. 6 and (d) Aug. 8 (For interpretation of the references to colour in this figure legend, the reader is referred to the web version of this article).

Fred Moshary: Conceptualization, Resources, Writing – review & editing.

Declaration of Competing Interest

The authors declare that they have no known competing financial interests or personal relationships that could have appeared to influence the work reported in this paper.

Data availability

Data will be made available on request.

Acknowledgements

This study is in part supported by the National Natural Science Foundation of China (No. 42105164), Guangdong Basic and Applied Basic Research Foundation (No. 2022A1515011078), the New York State Energy Research Development Authority (NYSERDA) (grant # 183869). Authors are thankful for the data product from New York State Department of Environmental Conservation (NYSDEC), Connecticut Department of Energy & Environmental Protection (CT DEEP), National Oceanic and Atmospheric Administration (NOAA) and National Aeronautics and Space Administration (NASA).The funding agencies have not reviewed the manuscript, and it does not necessarily reflect the views or policies of NYSERDA and other agencies.

Appendix A. Supplementary material

Supplementary data to this article can be found online at https://doi.org/10.1016/j.envint.2023.107887.

References

Benjamin, B.-S., Peter, H., 2011. Asian influence on surface ozone in the United States: A comparison of chemistry, seasonality, and transport mechanisms. J. Geophys. Res.

Brotzge, J.A., et al., 2020. A technical overview of the New York State Mesonet standard network. J. Atmos. Ocean. Technol. 37, 1827–1845. https://doi.org/10.1175/JTECHD-19-0220.

Coggon, M.M., Gkatzelis, G.I., McDonald, B.C., Gilman, J.B., Schwantes, R.H., Abuhassan, N., Aikin, K.C., Arendd, M.F., Berkoff, T.A., Brown, S.S., Campos, T.L., Dickerson, R.R., Gronoff, G., Hurley, J.F., Isaacman-Vanwertz, G., Koss, A.R., Li, M., McKeen, S.A., Moshary, F., Peischl, J., Pospisilova, V., Ren, X., Wilson, A., Wu, Y., Trainer, M., Warneke, C., 2021. Volatile Chemical Product Emissions Enhance Ozone and Modulate Urban Chemistry. Proc. Natl. Acad. Sci. 118 e2026653118.

Cooper, O.R., Parrish, D.D., Stohl, A., Trainer, M., Nédélec, P., Thouret, V., Cammas, J.P., Oltmans, S.J., Johnson, B.J., Tarasick, D., Leblanc, T., Mcdermid, I.S., Jaffe, D., Gao, R., Stith, J., Ryerson, T., Aikin, K., Campos, T., Weinheimer, A., Avery, M.A., 2010. Increasing springtime ozone mixing ratios in the free troposphere over western North America. Nature 463 (7279), 344–348. https://doi.org/10.1038/nature08708.

Couillard, M.H., Schwab, M.J., Schwab, J.J., Lu, C.H.S., Joseph, E., Stutsrim, B., Shrestha, B., Zhang, J., Knepp, T.N., Gronoff, G.P., 2021. Vertical Profiles of Ozone Concentrations in the Lower Troposphere Downwind of New York City During LISTOS 2018–2019. J. Geophys. Res. Atmos. 126 (23) https://doi.org/10.1029/2021JD035108.

De Young, R., Carrion, W., Ganoe, R., Pliutau, D., Gronoff, G., Berkoff, T., Kuang, S., 2017. Langley mobile ozone lidar: ozone and aerosol atmospheric profiling for air quality research. Appl. Opt. 56, 721–730.

Derwent, R.G., Stevenson, D.S., Collins, W.J., Johnson, C.E., 2004. Intercontinental transport and the origins of the ozone observed at surface sites in Europe. Atmos. Environ. 38 (13), 1891–1901.

Duvall, R., A. Clements, G. Hagler, A. Kamal, Vasu Kilaru, L. Goodman, S. Frederick, K. Johnson Barkjohn, I. VonWald, D. Greene, AND T. Dye. 2021. Performance Testing Protocols, Metrics, and Target Values for Ozone Air Sensors: Use in Ambient, Outdoor, Fixed Site, Non-Regulatory and Informational Monitoring Applications. U. S. EPA Office of Research and Development, Washington, DC, EPA/600/R-20/279. https://cfpub.epa.gov/si/si_public_record_Report.cfm?dirEntryId=350784&Lab=CEMM.

Emmons, L.K., Walters, S., Hess, P.G., Lamarque, J.-F., Pfister, G.G., Fillmore, D., et al., 2010. Description and evaluation of the model for ozone and related chemical tracers, version 4 (MOZART-4). Geosci. Model Dev. 3, 43–67. https://doi.org/10.5194/gmd-3-43-2010.

Gan, C., Wu, Y., Madhavan, B., Gross, B., Moshary, F., 2011. Application of active optical sensors to probe the vertical structure of the urban boundary layer and assess anomalies in air quality model PM2.5 forecasts. Atmos. Environ. 45 (37), 6613–6621.

Geng, F., Tie, X., Guenther, A., Li, G., Cao, J., Harley, P., 2011. Effect of isoprene emissions from major forests on ozone formation in the city of Shanghai. China. Atmos. Chem. Phys. 11 (20), 10449–10459.

Gronoff, G., Robinson, J., Berkoff, T., Swap, R., Farris, B., Schroeder, J., Halliday, H.S., Knepp, T., Spinei, E., Carrion, W., Adcock, E.E., 2019. A method for quantifying near range point source induced O3 titration events using Co-located Lidar and Pandora measurements. Atmos. Environ. 204, 43–52. https://doi.org/10.1016/j.atmosenv.2019.01.052.

Gronoff, G., Berkoff, T., Knowland, K., Lei, L., Shook, M., Fabbri, B., et al., 2021. Case study of stratospheric intrusion above Hampton, Virginia: Lidar-observation and modeling analysis. Atmos. Environ. 118498 https://doi.org/10.1016/j.atmosenv.2021.118498.

Guenther, A.B., Jiang, X., Heald, C.L., Sakulyanontvittaya, T., Duhl, T., Emmons, L.K., Wang, X., 2012. The model of emissions of gases and aerosols from nature version 2.1 (MEGAN2.1): an extended and updated framework for modelingbiogenic emissions. Geosci. Model Dev. 5, 1471e1492. https://doi.org/10.5194/gmd-5-1471-2012.

Gupta, M., Mohan, M., 2015. Validation of WRF/Chem model and sensitivity of chemical mechanisms to ozone simulation over megacity Delhi. Atmos. Environ. 122, 220–229. https://doi.org/10.1016/j.atmosenv.2015.09.039.

Han, Z., González-Cruz, J., Liu, H., et al., 2022. Observed sea breeze life cycle in and around NYC impacts on PBL and surface UHI and ozone patterns. Urban Clim. 42, 101109 https://doi.org/10.1016/j.uclim.2022.101109.

Judd, L.M., Al-Saadi, J.A., Szykman, J.J., Valin, L.C., Williams, D., 2020. Evaluating Sentinel-5P TROPOMI tropospheric NO2 column densities with airborne and Pandora spectrometers near New York City and Long Island Sound. Atmos. Meas. Tech. 13 (11), 6113–6140.

Karambelas, A., 2020. LISTOS: Toward a Better Understanding of New York City's Ozone Pollution Problem (An overview of the Long Island Sound Tropospheric Ozone Study). EM A&WMA, October 2020, https://pubs.awma.org/flip/EM-Oct-2020/karambelas.pdf.

Lin, M., Fiore, A.M., Horowitz, L.W., Cooper, O.R., Naik, V., Holloway, J., 2012. Transport of Asian ozone pollution into surface air over the western United States in spring. J. Geophys. Res. Atmos. 117 (D21).

Liu, X.H., Zhang, Y., Xing, J., Zhang, Q., Kai, W., Streets, D.G., Jang, C., Wang, W.X., Hao, J.M., 2010. Understanding of regional air pollution over China using CMAQ, part II. Process analysis and sensitivity of ozone and particulate matter to precursor emissions. Atmos. Environ. 44 (30), 3719–3727.

Liu, H., Zhang, M., Han, X., 2020. A review of surface ozone source apportionment in China. Atmos. Oceanic Sci. Lett. = Daqi-he-haiyang-kexue-kuaibao. 13 (5), 470–484. https://doi.org/10.1080/16742834.2020.1768025.

Luo, H., Yang, L., Yuan, Z., Zhao, K., Zhang, S., Duan, Y., Huang, R., Fu, Q., 2020. Synoptic condition-driven summertime ozone formation regime in Shanghai and the implication for dynamic ozone control strategies, 745141130 Sci. Total Environ.. https://doi.org/10.1016/j.scitotenv.2020.141130.

Ma, S., Tong, D., Lamsal, L., Wang, J., Zhang, X., Tang, Y., et al., 2021. Improving the predictability of high-ozone episodes through dynamic boundary conditions, emission refresh and chemical data assimilation during the Long Island Sound Tropospheric Ozone Study (LISTOS) field campaign. Atmos. Chem. Phys. 21, 16531–16553.

McClenny, W.A., Williams, E.J., Cohen, R.C., Stutz, J., 2002. Preparing to measure the effects of the NOx SIP call – methods for ambient air monitoring of NO, NO2, NOy, and individual NOz species. J. Air. Waste. Manage. 52, 542–562. https://doi.org/10.1080/10473289.2002.10470801.

Milford, J.B., Gao, D., Sillman, S., Blossey, P., Russell, A.G., 1994. Total reactive nitrogen (NOy) as an indicator of the sensitivity of ozone to reductions in hydrocarbon and NOx emissions. J. Geophys. Res. 99, 3533–3542.

Miller, Paul J., 2017. Retrospective and Future Analysis of Air Quality In and Downwind of New York City, DRAFT White Paper, available at ww.nescaum.org/documents/listos.

Münkel, C., Schäfer, K., Emeis, S., 2011. Adding confidence levels and error bars to mixing layer heights detected by ceilometer. Proc. SPIE 8177, 817708–1 – 817708–9.

Ninneman, M., Lu, S., Zhou, X.L., Schwab, J., 2020. On the Importance of Surface-Enhanced Renoxification as an Oxides of Nitrogen Source in Rural and Urban New York State. ACS Earth Space Chem. 4, 1985–1992. https://doi.org/10.1021/acsearthspacechem.0c00185.

Ou, J., Yuan, Z., Zheng, J., Huang, Z., Min, S., Li, Z., Huang, X., Hai, G., Louie, P., 2016. Ambient Ozone Control in a Photochemically Active Region: Short-Term Despiking or Long-Term Attainment? Environ. Sci. Technol. 50 (11).

Robinson, P.J., 2001. On the definition of a heat wave. J. Appl. Meteorol. Climatol. 40 (4), 762–775.

Shen, J., Wang, X.S., Li, J.F., Li, Y.P., Zhang, Y.H., 2011. Evaluation and intercomparison of ozone simulations by Models-3/CMAQ and CAMx over the Pearl River Delta. Sci. China (Chem.) 54, 1789–1800.

Sillman, S., He, D., 2002. Some theoretical results concerning O3-NOx-VOC chemistry and NOx-VOC indicators. J. Geophys. Res. Atmos. 107 (D22).

Stockwell, W.R., Middleton, P., Chang, J.S., Tang, X., 1990. The second generation regional acid deposition model chemical mechanism for regional air quality modeling. J. Geophys. Res. Atmos. 95, 16343–16367.

Tao, M.; Fiore, Arlene; Jin, X.; Schiferl, L., Commane, R.; Judd, L., et al. 2022. Investigating Changes in Ozone Formation Chemistry during Summertime Pollution Events over the Northeastern United States. Environ. Sci. & Tech., 10.1021/acs.est.2c02972.

Torres-Vazquez, A., Pleim, J., Gilliam, R., Pouliot, A.N.D.G., 2022. Performance Evaluation of the Meteorology and Air Quality Conditions From Multiscale WRF-CMAQ Simulations for the Long Island Sound Tropospheric Ozone Study (LISTOS). e2021JD035890 J. Geophy. Res.: Atmospheres 127 (5). https://doi.org/10.1029/2021JD035890.

Verstraeten, W.W., Neu, J.L., Williams, J.E., Bowman, K.W., Boersma, F.K., 2015. Rapid increases in tropospheric ozone production and export from China. Nat. Geosci.

Westervelt, D.M., Ma, C.T., He, M.Z., Fiore, A.M., Kinney, P.L., Kioumourtzoglou, M., Wang, S., Xing, J., Ding, D., Correa, G., 2019. Mid-21st century ozone air quality and health burden in China under emissions scenarios and climate change. Environ. Res. Lett. 14 (7), 74030. https://doi.org/10.1088/1748-9326/ab260b.

Wu, Y., Nehrir, A.R., Ren, X., Dickerson, R.R., Huang, J., Stratton, P.R., Gronoff, G., Kooi, S.A., Collins, J.E., Berkoff, T.A., Lei, L., Gross, B., Moshary, F., 2021. Synergistic aircraft and ground observations of transported wildfire smoke and its impact on air quality in New York City during the summer 2018 LISTOS campaign, 773145030 Sci. Total Environ.. https://doi.org/10.1016/j.scitotenv.2021.145030.

Xu, D., Yuan, Z., Wang, M., Zhao, K., Liu, X., Duan, Y., Fu, Q., Wang, Q., Jing, S., Wang, H., Zhao, X., 2022. Multi-factor reconciliation of discrepancies in ozone-precursor sensitivity retrieved from observation- and emission-based models, 158106952 Environ. Int.. https://doi.org/10.1016/j.envint.2021.106952.

Zelm, R.V., Preiss, P., Goethem, T.V., Dingenen, R.V., Huijbregts, M., 2016. Regionalized life cycle impact assessment of air pollution on the global scale: Damage to human health and vegetation. Atmos. Environ.

Zhang, J., Ninneman, M., Joseph, E., Schwab, M.J., Shrestha, B., Schwab, J.J., 2020. Mobile Laboratory Measurements of High Surface Ozone Levels and Spatial Heterogeneity During LISTOS 2018: Evidence for Sea Breeze Influence. J. Geophys. Res. Atmos. 125 (11) https://doi.org/10.1029/2019JD031961.

Zhao, K., Bao, Y., Huang, J., Wu, Y., Moshary, F., Arend, M., Wang, Y., Lee, X., 2019. A high-resolution modeling study of a heat wave-driven ozone exceedance event in New York City and surrounding regions, 199368–379 Atmos. Environ.. https://doi.org/10.1016/j.atmosenv.2018.10.059.

Zhao, K., Huang, J., Wu, Y., Yuan, Z., Wang, Y., Li, Y., Ma, X., Liu, X., Ma, W., Wang, Y., Zhang, X., 2021a. Impact of Stratospheric Intrusions on Ozone Enhancement in the Lower Troposphere and Implication to Air Quality in Hong Kong and Other South China Regions. J. Geophys. Res. Atmos. 126 (18) https://doi.org/10.1029/2020JD033955.

Zhao, K., Luo, H., Yuan, Z., Xu, D., Du, Y., Zhang, S., Hao, Y., Wu, Y., Huang, J., Wang, Y., Jiang, R., 2021b. Identification of close relationship between atmospheric oxidation and ozone formation regimes in a photochemically active region, 102373–383 J. Environ. Sci.-China.. https://doi.org/10.1016/j.jes.2020.09.038.

Zhao, K., Wu, Y., Yuan, Z., Huang, J., Liu, X., Ma, W., Xu, D., Jiang, R., Duan, Y., Fu, Q., Xu, W., 2022. Understanding the underlying mechanisms governing the linkage between atmospheric oxidative capacity and ozone precursor sensitivity in the Yangtze River Delta, China: A multi-tool ensemble analysis, 160107060 Environ. Int.. https://doi.org/10.1016/j.envint.2021.107060.

Zheng, B., Tong, D., Li, M., Liu, F., Hong, C., Geng, G., Li, H., Li, X., Peng, L., Qi, J., Yan, L., Zhang, Y., Zhao, H., Zheng, Y., He, K., Zhang, Q., 2018. Trends in China's anthropogenic emissions since 2010 as the consequence of clean air actions. Atmos. Chem. Phys. 18 (19), 14095–14111. https://doi.org/10.5194/acp-18-14095-2018.

Zhu, J., Liang, X.Z., 2013. Impacts of the Bermuda High on Regional Climate and Ozone over the United States. J. Climate. 26 (3), 1018–1032.